Infrared spectroscopic study of sulfate-bearing calcite from deep-sea bamboo coral

Etienne Balan, Julie Aufort, Sophie Pouillé, Marie Dabos, Marc Blanchard, Michele Lazzeri, Claire Rollion-Bard, Dominique Blamart

HAL Id: hal-02107464
https://hal.science/hal-02107464

Infrared spectroscopic study of sulfate-bearing calcite from deep-sea bamboo coral

Etienne BALAN[1,*], Julie AUFORT[1], Sophie POUILLÉ[1], Marie DABOS[1], Marc BLANCHARD[1], Michele LAZZERI[1], Claire ROLLION-BARD[2] and Dominique BLAMART[3]

[1] Sorbonne Universités – Institut de Minéralogie, de Physique des Matériaux et de Cosmochimie (IMPMC), UPMC Université Paris 06, UMR CNRS 7590, UMR IRD 206, MNHN, 4 Place Jussieu, 75252 Paris Cedex 05, France
*Corresponding author, e-mail: Etienne.Balan@impmc.upmc.fr

[2] Institut de Physique du Globe de Paris, Université Paris Diderot, Sorbonne Paris Cité, UMR7154 CNRS, 75005 Paris, France

[3] Laboratoire des Sciences du Climat et de l'Environnement, CEA-CNRS-UVSQ, Université Paris-Saclay, Domaine du CNRS, Bâtiment 12, 4 Avenue de la Terrasse, 91198 Gif-sur-Yvette, France

Abstract: The powder infrared spectra of a sulfate-bearing calcitic coral sample are recorded at room temperature in attenuated total reflectance (ATR) geometry and at low temperature in transmission geometry. The comparison of ATR spectra recorded with diamond or Ge crystal confirms that the width and the shape of the prominent absorption bands, related to CO_3 groups, are dominantly affected by macroscopic electrostatic interactions. In contrast, the temperature-dependence of the position and width of weak and narrow absorption bands, related to CO_3 or SO_4 groups, can be interpreted in terms of thermal expansion, anharmonic coupling, and local strain fluctuations. The three SO_4 stretching bands display a contrasted thermal behavior, the frequency of one of them increasing with temperature. Based on first-principles calculation, this unusual temperature dependence is traced back to the anisotropy of calcite thermal expansion. These results sustain the previously proposed atomic-scale model of sulfate in calcite and attest to a dominantly structural nature of sulfate in the investigated sample. Accordingly, structurally substituted sulfur in deep-sea calcitic bamboo coral could be used as proxy of seawater sulfate.

Key-words: infrared spectroscopy; biogenic carbonates; carbonate-associated sulfate; anharmonicity.

1. Introduction

Calcium carbonate minerals occur as major phases in sedimentary environments and correspond to the main lithospheric reservoir of carbon (Berner *et al.*, 1983). They are known to naturally incorporate chemical impurities at trace or minor concentration levels (*e.g.*, Bender *et al.*, 1975; Boyle, 1981; Morse & Bender, 1990). These impurities can bring important information on the physical–chemical parameters prevailing during their formation. For example, the concentration and isotopic composition of elements such as magnesium, strontium, boron, or sulfur are quantitatively used for paleoenvironmental reconstructions (*e.g.*, Graham *et al.*, 1982; Mitsuguchi *et al.*, 1996; Palmer *et al.*, 1998; Elderfield & Ganssen, 2000; Kampschulte & Strauss, 2004; Rüggeberg *et al.*, 2008). The presence of chemical impurities can also modify the pathways of crystal growth, the relative stabilities of polymorphs, the size and shape of mineral particles, as well as their elasticity and hardness (*e.g.*, Berner, 1975; Paquette & Reeder, 1995; De Yoreo &

Vekilov, 2003; Wasylenki *et al.*, 2005; Vavouraki *et al.*, 2008; Kunitake *et al.*, 2013; Long *et al.*, 2013; Côté *et al.*, 2015).

From a crystal-chemical perspective, incorporation of impurities in minerals can display various levels of complexity. Isovalent cationic substitutions are often described by considering the strain related to the insertion of a rigid ionic sphere into an elastic continuum (Blundy & Wood, 1994). Such model can be refined by explicitly considering the site relaxation, *i.e.*, the local changes in the crystal geometry around the impurity (*e.g.*, Reeder *et al.*, 1999). In contrast, heterovalent substitutions and incorporation of molecular species with stiff chemical bonds in a more compliant matrix potentially involve a greater variety of charge compensating mechanisms, coordination states and geometric arrangements (*e.g.*, Reeder *et al.*, 1994; Balan *et al.*, 2014, 2016). In biominerals, an additional complexity arises from their composite nature, involving variably ordered inorganic and organic phases (*e.g.*, Weiner & Dove, 2003; Erez, 2003; Allemand *et al.*, 2004). In this case, the occurrence of trace elements in host

crystal sites or in foreign nano-phases or molecules can appear as an open question and bears on their use as geochemical proxies.

Beside the determination of partition coefficients from controlled synthesis experiments (*e.g.*, Busenberg & Plummer, 1985) or the chemical analysis of extant biological species (*e.g.*, Takano, 1985; Vielzeuf *et al.*, 2013), spectroscopic and diffraction-based studies may help to unravel the incorporation mechanisms of impurities and to determine the modification of material properties caused by these impurities. Focusing on molecular impurities, chemically selective methods such as X-ray Absorption spectroscopy (Reeder *et al.*, 1994; Tang *et al.*, 2007; Branson *et al.*, 2015) and Nuclear Magnetic Resonance spectroscopy (Sen *et al.*, 1994; Klochko *et al.*, 2009; Rollion-Bard *et al.*, 2011; Mavromatis *et al.*, 2015; Noireaux *et al.*, 2015) have been used to determine the location and coordination states of selenate, chromate and borate in carbonate minerals. Infrared and Raman spectroscopy can also detect specific signals related to the internal vibrational modes of molecular groups (*e.g.*, Takano *et al.*, 1980; Takano, 1985; Riccardi, 2007; Fernández-Díaz *et al.*, 2010; Floquet *et al.*, 2015). These experimental studies can be sustained by molecular modeling approaches (*e.g.*, Fernández-Díaz *et al.*, 2010; Balan *et al.*, 2014, 2016; Arroyo-de Dompablo *et al.*, 2015), bringing straightforward relations between the spectroscopic properties, thermodynamic parameters, and atomic-scale arrangement of the trace molecular group in its crystalline host.

The present study focuses on the infrared spectroscopic properties and location of sulfate in biogenic calcite. Sulfate is a common impurity in carbonate minerals (Gill *et al.*, 2008). The sulfur isotopic composition of carbonate-associated sulfate is currently used as a proxy of the seawater sulfate isotopic composition (*e.g.*, Strauss, 1999; Kampschulte & Strauss, 2004; Riccardi *et al.*, 2006). It brings important information to infer the global balance between oxidized and reduced forms of sulfur over geological times (Halevy *et al.*, 2012). Sulfate groups also significantly affect the growth of carbonate-group minerals (Vavouraki *et al.*, 2008). The seawater sulfate concentration, together with Mg/Ca ratio, has been suggested as a key parameter controlling the preferential formation of aragonite *vs.* calcite in past oceans (Bots *et al.*, 2011). Numerous studies suggest that sulfate groups are structurally incorporated in carbonate minerals (Takano *et al.*, 1980; Pingitore *et al.*, 1995; Kontrec *et al.*, 2004; Vavouraki *et al.*, 2008; Vielzeuf *et al.*, 2013; Balan *et al.*, 2014; Tamenori *et al.*, 2014; Floquet *et al.*, 2015). Sulfate incorporation is easier in calcite than in aragonite and facilitated by the occurrence of Mg up to 2–3 wt% in calcite (Takano, 1985). However, other forms of sulfur, such as S-containing aminoacids and sulfated sugars, have also been observed to be associated to the organic fraction in biogenic carbonates (Cuif *et al.*, 2003; Dauphin *et al.*, 2005; Vielzeuf *et al.*, 2013; Tamenori *et al.*, 2014; Nguyen *et al.*, 2014; Floquet *et al.*, 2015).

Here, we analyze in details the infrared spectroscopic properties of a sulfate-bearing deep-sea calcitic coral (bamboo coral). Deep-sea corals have important geochemical implications because they potentially offer long-term records of ocean water-mass variability, related to climatic parameters fluctuations (Murray Roberts *et al.*, 2009). The Fourier-transform infrared (FTIR) spectrum is recorded at room temperature in attenuated total reflectance (ATR) geometry and its temperature-dependence is explored in transmission geometry. The present results show that the spectroscopic properties of the biogenic calcite, *i.e.*, the host crystalline matrix, can be interpreted in the light of the inorganic calcite properties whereas the temperature-dependence of the sulfate absorption spectrum brings a new support to the previously proposed structural model of sulfate in calcite (Balan *et al.*, 2014).

2. Analyzed sample

The analyzed sample is a deep-sea calcitic coral (bamboo coral; phylum Cnidaria, class Anthozoa, subclass Octocorallia, family Isidae) collected off the coast of Chile at around 77°E, 33°S at 500 m water depth during dredging operation. Optically clean fragments were selected under a binocular microscope and were gently ground in an agate mortar. Minor and trace element compositions were measured at Service d'Analyse des Roches et Minéraux (SARM) national facility (Nancy, France) following the method described in Carignan *et al.* (2001). They include Mg (3.0 wt% MgO), Na (0.45% Na_2O), Sr (2447 ppm), B (~100 ppm) and sulfate (~3000 ppm). The reproducibilities of major and trace element measurements are around ±2% and ±10%, respectively.

3. Infrared spectroscopic measurements

Infrared spectra were recorded using a Nicolet 6700 FTIR spectrometer equipped with an Ever-Glo source, KBr beamsplitter and DTGS-KBr detector. The spectra were obtained between 500 and 4000 cm^{-1} by averaging 100 scans with a resolution of 1 cm^{-1}. The room temperature ATR-FTIR spectrum was recorded on the sample powder packed at the surface of a diamond or Ge ATR crystal using a Quest ATR device (Specac). Low-temperature FTIR transmission measurements were performed on a composite pellet made of the calcite sample and a diluting KBr matrix. The pellet was obtained by compressing a mixture of about 10 mg of gently ground sample diluted in 300 mg of dried KBr under a pressure of 10^4 kg cm^{-2}. It was oven-dried overnight to remove adsorbed water, and pressed again at the same pressure before insertion in the high-vacuum chamber. During the measurements, the sample temperature was controlled using an ARS CS-204 SI cryocooler fitted with KRS-5 windows and a Si diode fixed on the sample holder. Measurements were collected from 10 to 290 K by steps of 40 K.

The position of the maximum of the bands was determined on the raw spectra. Accuracy on the position is estimated to be better than ±0.2 cm^{-1}. The analysis of the

width was performed using the autocorrelation method exposed in Salje *et al.* (2000) and further used in Blanch *et al.* (2007) and Balan *et al.* (2010, 2011). This method provides an efficient way to extract a robust width parameter Δ_{corr} from spectra displaying complex band shape and baseline, for which conventional fitting procedure using symmetric lorentzian or gaussian-type functions would lead to disputable results. It is particularly well suited to analyze the usually moderate changes of linewidths with temperature. For a simple lorentzian shape, the extracted autocorrelation parameter Δ_{corr} is close to its full-width at half maximum (FWHM).

4. Theoretical modeling

The sensitivity of vibrational modes to thermal expansion was theoretically assessed by computing the mode frequencies at selected cell geometries. Calculations were performed within density functional theory framework, using periodic boundary conditions and the generalized gradient approximation (GGA) to the exchange-correlation functional, as proposed by Perdew, Burke and Ernzerhof (PBE functional; Perdew *et al.*, 1996). The ionic cores were described using the latest version of ultra-soft pseudopotentials from the GBRV library (Garrity *et al.*, 2014). The electronic wave-functions and charge density were expanded using a finite basis set of plane-waves with 40 and 200 Ry cutoffs, respectively, corresponding to a convergence of the total energy better than $1\,mRy\,atom^{-1}$. The structural relaxation and vibrational mode calculations were performed using the PWscf and Phonon codes of the Quantum ESPRESSO package (Giannozzi *et al.*, 2009; http://www.quantum-espresso.org).

A periodic model of sulfate-bearing calcite was built from a rhombohedral $2 \times 2 \times 2$ super-cell of calcite (80 atoms) as in Balan *et al.* (2014). The geometry of the initial model was obtained by varying the internal coordinates to minimize the forces on atoms to less than $10^{-5}\,Ry\,a.u.^{-1}$, while the cell parameters were kept fixed to those of the theoretically relaxed pure calcite (hexagonal cell parameters: $a = 5.05$ Å, $c = 17.2$ Å). This initial model is assumed to correspond to the low-temperature ($T = 0$ K) structure of substituted sulfate in calcite. The temperature dependence was then considered by modifying the cell-parameters of the model using the experimentally determined variations of the calcite cell-parameters (Rao *et al.*, 1968). Two theoretical expanded geometries were considered by increasing the c cell-parameter by 0.25 and 0.5% and by using the corresponding experimentally determined variation of the c/a ratio. These two geometries correspond to a relative volume expansion of 0.16 and 0.33%, respectively, with an anti-correlated c cell-parameter increase and a cell-parameter decrease. Based on the linear variation of the cell-parameters as a function of temperature reported by Rao *et al.* (1967), they correspond to a temperature increase of ~84 and ~168 K, respectively. The two expanded models correspond to a homothetic expansion of the structure at $T = 0$ K, *i.e.*, internal

coordinates are kept fixed to those determined on the initial geometry without further minimizing the total energy of the system. For the three cell geometries (*i.e.*, $\Delta V/V_0 = 0$, 0.16 and 0.33%), harmonic frequencies of the SO_4 internal modes were calculated at the Brillouin zone center (Γ point) using the linear response theory (Baroni *et al.*, 2001). They were obtained by diagonalizing a partial dynamical matrix restricted to displacements of atoms belonging to the sulfate group only. As previously shown (Balan *et al.*, 2014), this approximation leads to SO_4 vibrational frequencies differing by less than $3\,cm^{-1}$ from those obtained from the full dynamical matrix.

5. Results and discussion

5.1. ATR spectrum of biogenic calcite

The ATR spectrum of the calcitic coral sample displays the absorption bands commonly observed in calcite (Fig. 1). A full interpretation of these bands has been given by, *e.g.*, Hellwege *et al.* (1970) and White (1974). The vibrational modes of calcite were also determined by theoretical calculations (*e.g.*, Pavese *et al.*, 1992; Prencipe *et al.*, 2004; Valenzano *et al.*, 2006). In the investigated frequency range, all the observed calcite bands correspond to the internal vibrational modes of the carbonate groups and can be related to those of the isolated CO_3 group, referred to as ν_1, ν_2, ν_3 and ν_4 (White, 1974). The ν_1 and ν_2 modes are not degenerated and correspond to the totally symmetric C–O stretching mode and to the oscillating motion of the C atom perpendicularly to the CO_3 plane, respectively. The degenerated ν_3 and ν_4 modes correspond to anti-symmetric C–O stretching and to bending modes, respectively.

The intense bands related to the ν_3 and ν_2 CO_3 modes are comparatively broader than the other absorption bands (Fig. 1a). In the diamond ATR spectrum, the ν_3 CO_3 band extends from about 1000 to $1490\,cm^{-1}$, while the ν_2 CO_3 band extends from about 840 to $890\,cm^{-1}$. Both bands display the peculiar asymmetric shape due to joint effects of the macroscopic electrostatic properties of the sample and experimental ATR geometry, as discussed in details by Aufort *et al.* (2016). Briefly, this shape can be understood by considering that the sample properties are well described by the effective dielectric properties of a solid/air composite obtained within the Bruggeman (1935) approach. In this case, the imaginary (absorptive) part of the dielectric function extends from the transverse to the longitudinal optical (LO) frequencies of the modes, explaining the asymmetry of the bands toward higher wavenumbers. For the ν_3 CO_3 and the less intense ν_2 CO_3 band of pure calcite, the experimental splitting between transverse optical (TO) and LO frequencies is $142\,cm^{-1}$ and $18\,cm^{-1}$, respectively (White, 1974). The relatively low refractive index of diamond ($n = 2.4$), although leading to a stronger absorbance and better signal/noise ratio than more refractive ATR crystals such as Ge ($n = 4$), induces additional modifications of the band shape with respect to the absorptive part of the sample dielectric function. They consist in a shift and a
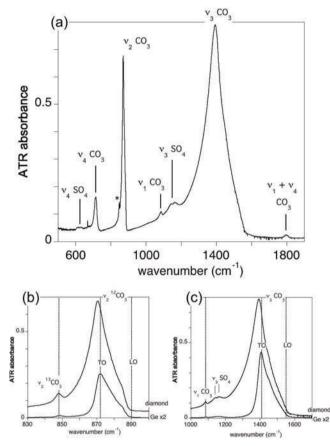
Fig. 1. (a) ATR-FTIR spectrum of biogenic calcite recorded using a diamond ATR crystal. At the bottom are shown enlarged views of the ν_2 CO$_3$ (b) and ν_3 CO$_3$ (c) bands comparing the ATR spectra recorded using diamond and Ge crystals. To facilitate the comparison, the intensity of the Ge ATR spectrum has been multiplied by two. The transverse optical (TO) and longitudinal optical (LO) frequencies of the ν_2 and the ν_3 CO$_3$ modes of pure calcite (White, 1974) are reported. Note the similar shape of the ν_2 and ν_3 CO$_3$ bands. The differences observed between the diamond and Ge ATR spectra attest to the role of macroscopic electrostatic effects on the band shapes. The weak band related to ^{13}CO$_3$ species (marked with an asterisk in (a)) and that related to the ν_1 CO$_3$ mode are not affected by these effects.

pronounced asymmetry toward lower wavenumbers. This is particularly apparent when comparing the diamond ATR spectrum with that obtained with a Ge crystal (Fig. 1b and c). The maximum of the ν_3 CO$_3$ band at 1393 cm^{-1} is shifted by about -14 cm^{-1} from the TO frequency of pure calcite, whereas this shift is only of -2 cm^{-1} for the ν_2 CO$_3$ band observed at 870.5 cm^{-1}. Thus, the two prominent ν_3 and ν_2 CO$_3$ absorption bands in the powder infrared spectrum of calcite are strongly affected by electrostatic effects. Because of their consequent broadening, they are not expected to provide detailed information on the atomic-scale structure of the sample. Similar conclusions were previously obtained for the intense bands in the powder infrared spectrum of apatite (Balan *et al.*, 2011; Aufort *et al.*, 2016).

The ν_1 and ν_4 CO$_3$ modes induce a smaller polarization of the crystal, as attested by smaller LO–TO splitting values (White, 1974). Therefore, they are less affected by

electrostatic interactions than the ν_3 and ν_2 CO$_3$ bands. They appear as weaker and narrower features in the spectrum (Fig. 1a) and can provide more information on microscopic (atomic-scale) structural parameters. The ν_1 CO$_3$ mode is not IR active in perfect calcite but is commonly observed as a weak band in natural and synthetic calcite samples (*e.g.*, Bottcher *et al.*, 1997; Xu & Poduska, 2014; Floquet *et al.*, 2015). In the investigated sample, it appears as an asymmetric band at 1085.5 cm^{-1}, overlapping with the low-frequency tail of the broad ν_3 CO$_3$ band. The observed asymmetry is related to this overlap, which induces a mixing between the imaginary and real parts of the dielectric function (Aufort *et al.*, 2016). The ν_4 CO$_3$ mode observed at 713.6 cm^{-1} is IR active but the corresponding experimental splitting of LO and TO modes is only of 3 cm^{-1} (White, 1974). In the investigated sample, its FWHM is significantly larger, amounting to $\sim$17 cm^{-1}. This indicates that electrostatic effects cannot represent a dominant contribution to its width and shape. Its position is consistent with the presence of Mg in the calcite structure (Bottcher *et al.*, 1997; Dauphin, 1999). A weak and narrow band is also observed at 848 cm^{-1} on the low-frequency side of the ν_2 CO$_3$ band. This weak feature is observed in various carbonate minerals and has been related to the ν_2 vibration of the ^{13}CO$_3$ isotopic species, which naturally occurs with an abundance of 1.1% (Sterzel & Chorinsky, 1968; Belousov *et al.*, 1970; White, 1974; Floquet *et al.*, 2015). However, it could also be related to a combination mode involving the ν_4 CO$_3$ mode and a lattice mode (Donoghue *et al.*, 1971; White, 1974; Carteret *et al.*, 2013). Several combination bands are observed at higher frequency. A combination of ν_1 and ν_4 modes is observed at 1797.9 cm^{-1}, while a combination of ν_1 and ν_3 modes is observed at 2518.2 cm^{-1}. This last value is consistent with the presence of Mg in the sample (Bottcher *et al.*, 1997).

The weak bands (Fig. 1a) observed at 611, 630, 1144.2 and 1163.2 cm^{-1} can be ascribed to internal vibrations of SO$_4$ groups (Takano *et al.*, 1980; Takano, 1985; Riccardi, 2007; Floquet *et al.*, 2015). The vibrations of an isolated SO$_4$ group with Td symmetry consist in two triply degenerated ν_3 (S–O stretching) and ν_4 (rocking) modes, a doubly degenerated ν_2 (scissoring) and a non-degenerated ν_1 (totally symmetric S–O stretching) mode. In the calcite structure, the degenerated modes are split by interaction with the host crystal structure (Balan *et al.*, 2014). The doublet at 611 and 630 cm^{-1} corresponds to ν_4 vibrations, whereas that at 1144.2 and 1163.2 cm^{-1} can be ascribed to ν_3 vibrations. The feature at 1248 cm^{-1} observed by Floquet *et al.* (2015) on a calcitic red coral sample is not present in the studied calcitic coral sample.

5.2. Low-temperature dependence of internal CO$_3$ modes in biogenic calcite

As discussed above, the temperature dependence of relatively weak and narrow bands is expected to bring more detailed information on microscopic order parameters than the broad prominent bands of the powder IR spectrum of calcite (*e.g.*, Xu & Poduska, 2014).

Accordingly, the signal/noise ratio of the weak absorption bands has been improved by increasing the calcite/KBr ratio of the sample measured in transmission geometry whereas the saturated strong ν_3 and ν_2 absorption bands were not analyzed.

The ν_4 and ν_1 CO_3 bands, as well as the ν_2 $^{13}CO_3$ feature, display small changes with temperature (Fig. 2). Their shift between 10 and 290 K is smaller than 1 cm^{-1} and the temperature dependence of their width is also weak.

The width parameter Δ_{corr} of the ν_4 and ν_2 $^{13}CO_3$ bands displays the temperature dependence typically ascribed to anharmonic coupling between the vibrational excitation and other vibrational modes of the structure (*e.g.*, Menéndez & Cardona, 1984): it consists in a low-temperature quantum saturation domain in which the linewidth is almost temperature-independent followed by a marked increase in the linewidth at higher temperature (Fig. 2). This behavior relates to the decay of the excitation in two phonons and can be fitted using an equation of the form (Salje *et al.*, 1991; Blanchard *et al.*, 2014):

$$A(T) = A_0 + B \coth(\theta_S/T) \qquad (1)$$

where T is the temperature (K) and A_0, B and θ_S are adjustable parameters. In this formalism, the temperature-independent domain extends from 0 K to a critical temperature $T_s \sim \theta_S/2$. Previous investigations of the temperature dependence of the calcite vibrational spectrum have shown that four-phonon processes can also contribute to the homogeneous broadening of the bands (Sakurai & Sato, 1971; Sood *et al.*, 1981; Delfyett *et al.*, 1989). Notably, four-phonon processes lead to the phase relaxation of the vibrational excitation by phonon-phonon scattering. Three- and four-phonon processes could be discriminated by their different temperature dependence but this would require investigations at higher temperatures than in the present study (Sakurai & Sato, 1971) or dedicated experiments (Delfyett *et al.*, 1989). Accordingly, we restrict our analysis to the generic ansatz given by Eq. (1).

For the ν_4 and ν_2 $^{13}CO_3$ bands, the variation of the linewidth with temperature does not exceed 0.2 cm^{-1} in the investigated range (Fig. 2). This indicates that, beside the instrumental resolution ($\sim$1 cm^{-1}), the observed width is mostly determined by inhomogeneous broadening contributions. These contributions include macroscopic electrostatic interactions and the dependence of vibrational frequencies on local strain fluctuations. The electrostatic contribution should be negligible for the ν_2 $^{13}CO_3$ band which is related to a highly dilute species. The ν_2 $^{13}CO_3$ mode also displays a very small dependence on variations in the crystal cell geometry, as attested by the theoretical analysis of Gueta *et al.* (2007) and observations on the isostructural mineral magnesite (Grzechnik *et al.*, 1999; Clark *et al.*, 2011). Consequently, the ν_2 $^{13}CO_3$ band displays a very small width parameter at 0 K ($\Delta_{corr} \sim 2.6$ cm^{-1}). For the ν_4 band, the electrostatic contribution would not exceed 3 cm^{-1}, corresponding to the LO–TO

splitting value. Its more significant width ($\sim$11 cm^{-1}) thus attests for a significant distribution in the environment of carbonate groups. In biogenic minerals, local strain fluctuations may arise from the incorporation of chemical impurities and finite size effects. In the case of calcitic coral, Mg and sulfate incorporation are expected to play a major role in the fluctuations of the local environment of CO_3 groups (Floquet *et al.*, 2015).

The position of the ν_4 and ν_2 $^{13}CO_3$ bands also displays a quantum saturation domain at low temperature followed by a more pronounced shift above a critical temperature (Fig. 2; Table 1). Compared with the linewidth, the mode frequency variation contains an additional contribution related to the thermal expansion of the crystal structure (Menéndez & Cardona, 1984; Lazzeri *et al.*, 2003). In calcite, this contribution is however expected to be significantly smaller (Sakurai & Sato, 1971). Here, we note that the results obtained on the ν_2 $^{13}CO_3$ band are well consistent with those reported by Sakurai & Sato (1971) for the ν_2 $^{12}CO_3$ mode of a single crystal of optical-grade natural calcite, *i.e.*, a damping coefficient at 300 K of 1.9 cm^{-1} (to be compared to $\Delta_{corr} = 2.8$ cm^{-1} at 290 K in the present study) and an anharmonic shift of 0.3 cm^{-1} (to be compared to 0.4 cm^{-1} at 290 K in the present study). This agreement further confirms the very small sensitivity of the ν_2 CO_3 mode to variations of its local environment (Gueta *et al.*, 2007). It is fully consistent with the interpretation of this band as related to the $^{13}CO_3$ species, instead of to a two-phonon absorption. A significantly different behavior and a larger linewidth would be expected in the case of a combination band involving low-frequency vibrational modes.

The behavior of the ν_1 CO_3 band (Fig. 2) is not easily explained within the same framework. Its position shows a linear variation with temperature without perceptible low-temperature saturation domain. The corresponding slope is -3.6×10^{-3} cm^{-1} K^{-1} (Table 1). Its width parameter displays a low-temperature saturation domain with relatively dispersed values but it is followed by a decrease with increasing temperature. This variation of the width of the ν_1 CO_3 band cannot be simply related to anharmonic phonon decay, which tends to decrease the phonon lifetime (thus increasing the linewidth) with increasing temperature (Delfyett *et al.*, 1989). The observed behavior should thus arise from a temperature-related change in the inhomogeneous broadening of the band. The ν_1 CO_3 band displays two characteristics that could be linked to its anomalous behavior. The observed absorption is indeed exclusively related to a break of the IR selection rules, most likely induced by local distortions of the structure. In addition, it overlaps with the low frequency tail of the strong ν_3 CO_3 band. As discussed for the ATR spectrum, this overlap leads to a marked asymmetric shape depending on the respective contribution and position of the narrow and broad resonances (Aufort *et al.*, 2016). Whatever its precise origin, the overall change of the width with temperature remains small, typically within 0.2 cm^{-1}. As for the ν_4 CO_3 band, the observed width should be mostly related to local strain fluctuations. Both bands
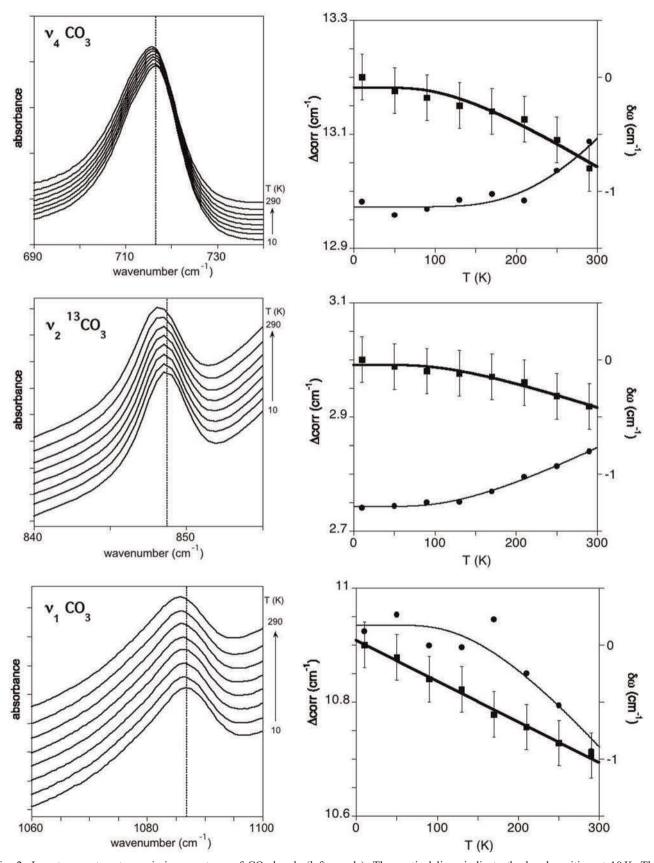
Fig. 2. Low-temperature transmission spectrum of CO_3 bands (left panels). The vertical lines indicate the band position at 10 K. The temperature dependence of the position $\delta\omega = \omega - \omega_0$ (squares, bold curves) and width Δ_{corr} (circles) parameters are reported in the right panels. Note the quantum saturation observed at low temperature for the ν_4 and ν_2 $^{13}CO_3$ bands. The width parameter has been determined after a linear baseline subtraction on the following domains 680–735 cm^{-1} (ν_4 CO_3), 840–852 cm^{-1} (ν_2 $^{13}CO_3$), 1060–1098 cm^{-1} (ν_1 CO_3). The parameters of the fits using Eq. (1) are reported in Table 1.

Table 1. Temperature-dependence of position and width of selected CO_3 and SO_4 bands. Measurements are fit with Eq. (1), which defines the quantities A_0, B, T_S. The average slope of the frequency ω and of the width parameter (Δ_{corr}, defined in Salje *et al.*, 2000) as a function of temperature, $d\omega/dT$ and $d(\Delta_{corr})/dT$, respectively, are also reported.

Band	Position					Width			
	ω_0 (10 K) (cm^{-1})	A_0 (cm^{-1})	B (cm^{-1})	θ_S (K)	$d\omega/dT$ (cm^{-1}K^{-1})	A_0 (cm^{-1})	B (cm^{-1})	θ_S (K)	$d(\Delta_{corr})/dT$ (cm^{-1}K^{-1})
ν_4 CO$_3$	716.4	0.85	−0.95	197	–	11.4	1.6	496	–
ν_2 ^{13}CO$_3$	848.7	0.45	−0.49	194	–	2.6	0.17	221	–
ν_1 CO$_3$	1086.8	–	–	–	-3.6×10^{-3}	11.4*	−0.5*	260*	–
ν_4 SO$_4$ (A)	611.8	–	–	–	<d.l.	12.0	–	–	5.2×10^{-3}
(B)	631.8	6.7	−6.7	347	–	"	–	–	"
ν_3 SO$_4$ (C)	1142.9	–	–	–	6.6×10^{-3}	27.7	–	–	44.1×10^{-3}
(D)	1168.2	–	–	–	-12.6×10^{-3}	"	–	–	"
(E)	1175.8	–	–	–	n.d.	"	–	–	"

* The fitting parameters of the ν_1 CO$_3$ width are not related to anharmonicity (see text).

indeed display comparable width (Table 1) and the related modes have a similar sensitivity to pressure changes (Salje & Viswanathan, 1976; Clark *et al.*, 2011).

5.3. Low-temperature dependence of internal SO$_4$ modes in biogenic calcite

The room-temperature spectrum (Fig. 1a) of the sample displays four bands which can be ascribed to the ν_4 and ν_3 SO$_4$ vibrations. In the spectrum recorded at 10 K, the bands at 611.8 and 631.8 cm^{-1} (labeled A and B in Fig. 3), as well as an additional broad feature observed at 673 cm^{-1}, can be ascribed to the triply degenerated ν_4 vibration split by the interaction of the molecular species with the crystalline host. The three bands related to the split ν_3 vibration are observed at 1142.9, 1162.8 and 1175.8 cm^{-1} (bands C, D and E in Fig. 3). A very weak feature is observed at 1021 cm^{-1} corresponding to the ν_1 band. The ν_4 band at 612 cm^{-1} (band A) does not display any apparent shift with temperature, whereas that at 631.5 cm^{-1} (band B) shows a slight frequency decrease with temperature, analogous to that observed for the ν_4 and ν_2 ^{13}CO$_3$ bands. Its θ_S value of 347 K corresponds to a coupling with a mode at $\sim$241 cm^{-1}, thus enabling an efficient decay toward the low-frequency domain of the calcite density of vibrational states (Catti *et al.*, 1993). A more contrasted behavior is observed among the ν_3 SO$_4$ stretching bands. The band C at 1142.9 cm^{-1} shifts toward the high frequency values with increasing temperature; whereas the two other bands display a marked shift toward the lower frequencies (Fig. 2). The position of the high-frequency band E at 1175.8 cm^{-1} could not be determined over the whole temperature range because of its overlap with band D when the temperature increases. For the three bands, the magnitude of the shifts is significantly larger than that observed for the CO$_3$ modes and the ν_4 SO$_4$ bands (Figs. 2 and 3). The overall width parameter Δ_{corr} determined for the two bands A and B displays an increase of $\sim$2 cm^{-1} with temperature, whereas its increase for the three ν_3 bands reaches 14 cm^{-1}. In both cases, the width parameter is affected by variations in the line splitting and related band overlaps.

Insight in the origin of the observed lineshift can be obtained by considering the theoretical variation of the vibrational frequencies of the SO$_4$ group as a function of crystal thermal expansion. The theoretical model of SO$_4$ in calcite (Fig. 4) is identical to that previously obtained by Balan *et al.* (2014). The SO$_4$ group is slightly tilted with one S–O bond approximately oriented along the *c*-axis (S–O1), two S–O bonds in the perpendicular plane (S–O2 and S–O4) and the last S–O3 bond with an intermediate orientation. A full modeling of the temperature-dependent vibrational properties of the system would require minimization of its free-energy as a function of internal coordinates at a given temperature, using *e.g.*, the quasi-harmonic approximation (Catti *et al.*, 1993; Quong & Liu, 1997; Lazzeri & de Gironcoli, 1998). This approach requires extensive calculation of the phonon density of states and is hardly applicable to large system sizes, such as those considered in the present study. For this reason, a simplified approach is used. It consists in calculating the harmonic vibrational frequencies of SO$_4$ groups for systems obtained by a homothetic expansion of the cell geometry (clamped atomic positions). All inter-atomic bonds are thus considered to deform in a similar way. The frequency variations related to rigid molecular groups (*e. g.*, CO$_3$, SO$_4$) are likely to be overestimated with respect to those related to vibration of softer bonds (*e.g.*, Ca–O). Meanwhile, a reasonable account of the contrasted behavior of the modes with a similar nature, such as the S–O stretching modes, is expected. We also recall that anharmonic frequency shift results from a sum of a lattice thermal expansion contribution and of the direct phonon-phonon anharmonic interactions as described in Menéndez & Cardona (1984). The present approach only considers the first contribution.

As previously observed (Balan *et al.*, 2014), the theoretical frequencies of internal SO$_4$ vibrational modes are underestimated by $\sim$5% (Table 2). This underestimation is ascribed to the usual overestimation of bond lengths and underestimation of corresponding force constants by the GGA. All the ν_4 modes display a small frequency lowering when the crystal cell expands, with the low-frequency mode
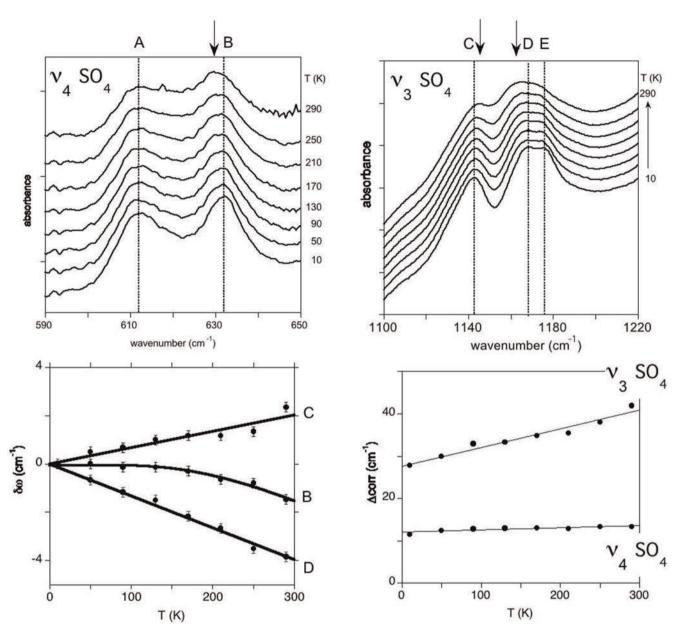
Fig. 3. Low-temperature transmission spectra of SO_4 bands (top panels). Note the contrasted shift of bands B, C and D (left bottom panel). Global width parameters Δ_{corr} (right bottom panel) have been determined after a linear baseline subtraction on the domain 590–650 cm^{-1} (ν_4 SO_4) and a non-linear Stineman baseline (Stineman, 1980) on the domain 1100–1220 cm^{-1} (ν_3 SO_4). The parameters of the fits using Eq. (1) for band B and linear behavior for the other curves are reported in Table 1. The vertical lines indicate the band position at 10 K, whereas the vertical arrows point to the position of shifted bands at room temperature.

displaying the weakest dependence. This behavior is consistent with the contrasted shifts experimentally observed for the two bands A and B. A more contrasted behavior is predicted by calculations for the stretching modes (Table 2; Fig. 4). The mode computed at 1073 cm^{-1}, corresponding to the band C (Fig. 3), is mostly related to the coupled stretching vibration of the S–O2 and S–O4 bonds. It displays a frequency increase as a function of the crystal cell expansion. In contrast, the mode calculated at 1109.9 cm^{-1}, corresponding to band D, is related to the S–O3 stretching vibration. It displays a moderate decrease as a function of the crystal cell expansion. Finally, the mode calculated at 1153.8 cm^{-1}, corresponding to band E, is related to the

S–O1 stretching and displays a strong and likely over-estimated dependence on the crystal cell geometry. Thus, the simple theoretical assessment of the dependence of vibrational frequencies of the SO_4 group on the cell parameters is consistent with the contrasted behavior measured for the experimental ν_3 SO_4 bands, and more specifically with the positive shift of the lowest frequency ν_3 SO_4 band (band B) as a function of temperature. This contrasted behavior can be traced back to the anisotropy of the crystal expansion, which corresponds to a decrease of the a cell-parameter and concomitant increase of the c cell-parameter (Rao *et al.*, 1968). Accordingly, the shift of the ν_3 SO_4 bands in calcite seems to be mostly related to the
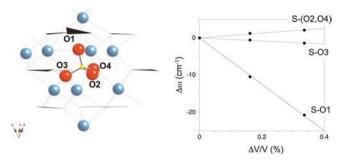
Fig. 4. Model of sulfate substituted for carbonate in calcite (after Balan *et al.*, 2014). The three-fold axis of the structure is vertically oriented. The carbonate groups correspond to the black triangles. The S atom is in yellow, calcium atoms in blue, oxygen atoms in red. The calculated dependence of vibrational S–O stretching frequencies (ν_3 SO$_4$) on crystal cell expansion is reported on the right. Note the contrasted behavior of the three modes, depending on the structural orientation of the corresponding S–O bonds. (Online version in color.)

Table 2. Sulfate mode frequencies and their dependence on crystal cell volume. Measurements (exp) *vs.* calculations (theo). The parameter V_0 ($\Delta\omega/\Delta V$) corresponds to the frequency variation as a function of relative cell-volume change.

Mode	ω_{theo} (cm^{-1})	V_0 ($\Delta\omega/\Delta V$) (theory) (cm^{-1})	ω_{exp} (cm^{-1})
ν_4 SO$_4$	587.8	−130	611.8 (A)
	592.9	−260	631.8 (B)
	632.9	−310	673.0
ν_1 SO$_4$	962.7	−820	1021.0
ν_3 SO$_4$	1073.1 (S–(O2,O4))	+660	1142.9 (C)
	1109.9 (S–O3)	−410	1168.2 (D)
	1153.8 (S–O1)	−6230	1175.8 (E)

Note: The dominant contribution of S–O bonds for the ν_3 SO$_4$ modes are indicated in parenthesis. Oxygen labels refer to Fig. 4.

thermal expansion of the structure, with a weaker role of phonon-phonon anharmonic coupling between the localized vibrational modes and the vibrational density of states of the crystal host. This behavior differs from that of the CO$_3$ groups. In the case of the high-frequency modes of a molecular impurity in a crystal host, the number of anharmonic decay channels can be small, leading to weaker anharmonic effects at low temperature.

5.4. Concluding remarks

The combination of spectroscopic and molecular modeling tools appears as a powerful approach to unravel the status of chemical impurities in complex samples, such as biominerals. More specifically, the investigation of the low-temperature dependence of vibrational bands is expected to provide pertinent information about the dynamic interactions of molecular impurities with their crystalline host (Yi *et al.*, 2013). Interestingly, the anharmonic behavior observed on carbonate modes is well consistent with that previously observed on highly ordered calcite crystals, suggesting that the substantial

occurrence of Mg and sulfate impurities in the biogenic sample only has a moderate effect on mode-coupling parameters.

The comparison of experimental and theoretical results validates the atomic-scale model proposed for the sulfate incorporation at the carbonate site of the calcite structure. It further confirms the structural location of sulfate in deep-sea calcitic coral. According to the infrared spectroscopic observations, sulfate ions in deep-sea bamboo coral mainly substitutes for carbonate ion and the occurrence of S linked to the presence of organic matter (*e.g.*, Dauphin & Cuif, 1999; Cuif *et al.*, 2003; Dauphin *et al.*, 2005) plays a lesser role. One consequence is that the observation of S in deep-sea bamboo coral is not a reliable proxy of the presence of S-bearing organic molecules. On the contrary, sulfur as structurally substituted sulfur (SSS; Kampschulte & Strauss, 2004) in deep-sea calcitic bamboo coral could be used as proxy of seawater sulfate.

References

Allemand, D., Ferrier-Pages, C., Furla, P., Houlbreque, F., Puverel, S., Reynaud, S., Tambutte, E., Tambutte, S., Zoccola, D. (2004): Biomineralisation in reef-building corals: from molecular mechanisms to environmental control. *C.R. Palevol*, **3**, 453–467.

Arroyo-de Dompablo, M.E., Fernández-Gonzalez, M.A., Fernández-Diaz, L. (2015): Computational investigation of the influence of tetrahedral oxoanions (sulphate, selenate and chromate) on the stability of calcium carbonate polymorphs. *RSC Adv.*, **5**, 59845.

Aufort, J., Ségalen, L., Gervais, C., Brouder, C., Balan, E. (2016): Modeling the attenuated total reflectance infrared (ATR-FTIR) spectrum of apatite. *Phys. Chem. Minerals*, **43**, 615–626.

Balan, E., Delattre, S., Guillaumet, M., Salje, E.K.H. (2010): Low-temperature infrared spectroscopic study of OH stretching modes in kaolinite and dickite. *Am. Mineral.*, **95**, 1257–1266.

Balan, E., Delattre, S., Roche, D., Segalen, L., Morin, G., Guillaumet, M., Blanchard, M., Lazzeri, M., Brouder, C., Salje, E.K.H. (2011): Line-broadening effects in the powder infrared spectrum of apatite. *Phys. Chem. Minerals*, **38**, 111–122.

Balan, E., Blanchard, M., Pinilla, C., Lazzeri, M. (2014): First-principles modeling of sulfate incorporation and ^{34}S/^{32}S isotopic fractionation in different calcium carbonates. *Chem. Geol.*, **374–375**, 84-91.

Balan, E., Pietrucci, F., Gervais, C., Blanchard, M., Schott, J., Gaillardet, J. (2016): First-principles study of boron speciation in calcite and aragonite. *Geochim. Cosmochim. Acta*, **193**, 119–131.

Baroni, S., de Gironcoli, S., Dal Corso, A., Giannozzi, P. (2001): Phonons and related crystal properties from density-functional perturbation theory. *Rev. Modern Phys.*, **73**, 515–561.

Belousov, M.V., Pogarev, D.E., Shultin, A.A. (1970): Band intensity of extraplanar n$_2$ vibration of CO$_3{}^{2-}$ and NO$_3{}^-$ ions in crystals having calcite and aragonite structure. *Sov. Phys. Solid State*, **11**, 2185–2186.

Bender, M.L., Lorens, R.B., Williams, D.F. (1975): Sodium, magnesium, and strontium in the tests of planktonic foraminifera. *Micropaleontology*, **21**, 448–459.

Berner, R.A. (1975): The role of magnesium in the crystal growth of calcite and aragonite from sea water. *Geochim. Cosmochim. Acta*, **39**, 489–504.

Berner, R.A., Lasaga, A.C., Garrels, R.M. (1983): The carbonate-silicate geochemical cycle and its effect on atmospheric carbon dioxide over the past 100 million years. *Am. J. Sci.*, **283**, 641–683.

Blanch, A.J., Quinton, J.S., Lenehan, C.E., Pring, A. (2007): Autocorrelation infrared analysis of mineralogical samples: the influence of user controllable experimental parameters. *Anal. Chim. Acta*, **590**, 145–150.

Blanchard, M., Balan, E., Giura, P., Béneut, K., Yi, H., Morin, G., Pinilla, C., Lazzeri, M., Floris, A. (2014): Infrared spectroscopic properties of goethite: anharmonic broadening, long-range electrostatic effects and Al substitution. *Phys. Chem. Minerals*, **41**, 289–302.

Blundy, J. & Wood, B. (1994): Prediction of crystal-melt partition coefficients from elastic moduli. *Nature*, **372**, 452–454.

Bots, P., Benning, L.G., Rickaby, R.E.M., Shaw, S. (2011): The role of SO$_4$ in the switch from calcite to aragonite seas. *Geology*, **39**, 331–334.

Bottcher, M.E., Gehlken, P.L., Steele, D.F. (1997): Characterization of inorganic and biogenic magnesian calcites by Fourier transform infrared spectroscopy. *Solid State Ionics*, **101**, 1379–1385.

Boyle, E.A. (1981): Cadmium, zinc, copper, and barium in foraminifera tests. *Earth Planet. Sci. Lett.*, **53**, 11–35.

Branson, O., Kaczmarek, K., Refern, S.A.T., Misra, S., Langer, G., Tyliszczak, T., Bijma, J., Elderfield, H. (2015): The coordination and distribution of B in foraminiferal calcite. *Earth Planet. Sci. Lett.*, **416**, 67–72.

Bruggeman, D.A.G. (1935): Berechnung verschiedener physikalischer Konstanten von heterogenen Substanzen. I. Dielektrizitätskonstanten und Leitfähigkeiten der Mischkörper aus isotropen Substanzen. *Ann. Phys.*, **416**, 665–679.

Busenberg, E. & Plummer, L.N. (1985): Kinetic and thermodynamic factors controlling the distribution of SO$_4{}^{2-}$ and Na$^+$ in calcites and selected aragonites. *Geochim. Cosmochim. Acta*, **49**, 713–725.

Carignan, J., Hild, P., Mevelle, G., Morel, J., Yeghicheyan, D. (2001): Routine analyses of trace elements in geological samples using flow injection and low pressure on-line liquid chromatography coupled to ICP-MS: a study of geochemical reference materials BR, DR-N, UB-N, AN-G and GH. *Geostand. Newsl.*, **25**, 187–198.

Carteret, C., De La Pierre, M., Dossot, M., Pascale, F., Erba, A., Dovesi, R. (2013): The vibrational spectrum of CaCO$_3$ aragonite: a combined experimental and quantum-mechanical investigation. *J. Chem. Phys.*, **138**, 014201.

Catti, M., Pavese, A., Price, G.D. (1993): Thermodynamic properties of CaCO$_3$ calcite and aragonite: a quasi-harmonic calculation. *Phys. Chem. Minerals*, **19**, 472–479.

Clark, S.J., Jouanna, P., Haines, J. Mainprice, D. (2011): Calculation of infrared and Raman vibration modes of magnesite at high pressure by density-functional perturbation theory and comparison with experiments. *Phys. Chem. Minerals*, **38**, 193–202.

Côté, A.S., Darkins, R., Duffy, D.M. (2015): Deformation twinning and the role of amino acids and magnesium in calcite hardness from molecular simulation. *Phys. Chem. Chem. Phys.*, **17**, 20178–20184.

Cuif, J.P., Dauphin, Y., Doucet, J., Salome, M., Susini, J. (2003): XANES mapping of organic sulfate in three scleractinian coral skeletons. *Geochim. Cosmochim. Acta*, **67**, 75–83.

Dauphin, Y. (1999): Infrared spectra and elemental composition in recent biogenic calcites: Relationships between the ν_4 band wavelength and Sr and Mg concentrations. *Appl. Spectrosc.*, **53**, 184–190.

Dauphin, Y. & Cuif, J.P. (1999): Relation entre les teneurs en soufre des biominéraux calcaires et leurs caractéristiques minéralogiques. *Ann. Sci. Nat.*, **2**, 73–85.

Dauphin, Y., Cuif, J.P., Salome, C., Susini, J. (2005): Speciation and distribution of sulfur in a mollusk shell as revealed by in situ maps using X-ray absorption near-edge structure (XANES) spectroscopy at the S K-edge. *Am. Mineral.*, **90**, 1748–1758.

Delfyett, P.J., Dorsinville, R., Alfano, R.R. (1989): Multiphonon dephasing of the 1086-cm^{-1} mode in calcite. *Phys. Rev. B: Condens. Matter*, **39**, 3845–3853.

De Yoreo, J.J. & Vekilov, P.G. (2003): Principles of crystal nucleation and growth. *in* "Biomineralization", P.M. Dove, J.J. De Yoreo, S. Weiner, eds. Mineralogical Society of America, Washington, D.C., Vol. 54.

Donoghue, M., Hepburn, P.H., Ross, S.D. (1971): Factors affecting the infrared spectra of planar anions with D3h, symmetry V: the origin of the splitting of the out-of-plane bending mode in carbonates and nitrates. *Spectrochim. Acta, A: Mol. Biomol. Spectrosc.*, **27**, 1065–1072.

Elderfield, H. & Ganssen, G. (2000): Past temperature and delta^{18}O of surface ocean waters inferred from foraminiferal Mg/Ca ratios. *Nature*, **405**, 442–445.

Erez, J. (2003): The source of ions for biomineralization in foraminifera and their implications for paleoceanographic proxies, biomineralization. *Rev. Mineral. Geochem.*, **54**, 115–149.

Fernández-Díaz, L., Fernández-González, A., Prieto, M. (2010): The role of sulfate groups in controlling CaCO$_3$ polymorphism. *Geochim. Cosmochim. Acta*, **74**, 6064–6076.

Floquet, N., Vielzeuf, D., Ferry, D., Ricolleau, A., Heresanu, V., Perrin, J., Laporte, D., Fitch, A.N. (2015): Thermally induced modifications and phase transformations of red coral Mg-calcite skeletons from infrared spectroscopy and high resolution synchrotron powder diffraction analyses. *Cryst. Growth Des.*, **15**, 3690–3706.

Garrity, K.F., Bennett, J.W., Rabe, K.M., Vanderbilt, D. (2014): Pseudopotentials for high-throuhput DFT calculations. *Comput. Mat. Sci.*, **81**, 446–452.

Giannozzi, P., Baroni, S., Bonini, N., Calandra, M., Car, R., Cavazzoni, C., Ceresoli, D., Chiarotti, G.L., Cococcioni, M., Dabo, I., Dal Corso, A., de Gironcoli, S., Fabris, S., Fratesi, G., Gebauer, R., Gerstmann, U., Gougoussis, C., Kokalj, A., Lazzeri, M., Martin-Samos, L., Marzari, N., Mauri, F., Mazzarello, R., Paolini, S., Pasquarello, A., Paulatto, L., Sbraccia, C., Scandolo, S., Sclauzero, G., Seitsonen, A.P., Smogunov, A., Umari, P., Wentzcovitch, R.M. (2009): Quantum ESPRESSO: a modular and open-source software project for quantum simulations of materials. *J. Phys.: Condens. Matter*, **21**, 395502.

Gill, B.C., Lyons, T.W., Frank, T.D. (2008): Behavior of carbonate-associated sulfate during meteoric diagenesis and implications for the sulfur isotope paleoproxy. *Geochim. Cosmochim. Acta*, **72**, 4699–4711.

Graham, D.W., Bender, M.L., Williams, D.F., Keigwin, L.D. (1982): Strontium-calcium ratios in Cenozoic planktonic foraminifera. *Geochim. Cosmochim. Acta*, **46**, 1281–1292.

Grzechnik, A., Simon, P., Gillet, P., McMillan, P. (1999): An infrared study of $MgCO_3$ at high pressure. *Phys. B: Condens. Matter*, **262**, 67–73.

Gueta, R., Natan, A., Addadi, L., Weiner, S., Refson, K., Kronik, L. (2007): Local atomic order and infrared spectra of biogenic calcite. *Angew. Chem. Int. Ed.*, **46**, 291–294.

Halevy, I., Peters, S.E., Fischer, W.W. (2012): Sulfate burial constraints on the Phanerozoic sulfur cycle. *Science*, **337**, 331–334.

Hellwege, K.H., Lesch, W., Plihal, M., Schaack, G. (1970): Zwei-phononen-absorptionsspektren und Dispersion der Schwingungszweige in Kristallen der Kalkspatstruktur. *Z. Phys.*, **232**, 61–86.

Kampschulte, A. & Strauss, H. (2004): The sulfur isotopic evolution of Phanerozoic seawater based on the analysis of structurally substituted sulfate in carbonates. *Chem. Geol.*, **204**, 255–286.

Klochko, K., Cody, G.D., Tossell, J.A., Dera, P., Kaufman, A.J. (2009): Re-evaluating boron speciation in biogenic calcite and aragonite using ^{11}B MAS NMR. *Geochim. Cosmochim. Acta*, **73**, 1890–1900.

Kontrec, J., Kralj, D., Brecevic, L., Falini, G., Fermani, S., Noethig-Laslo, V., Mirosavljevic, K. (2004): Incorporation of inorganic anions in calcite. *Eur. J. Inorg. Chem.*, **23**, 4579–4585.

Kunitake, M.E., Mangano, L.M., Peloquin, J.M., Baker, S.P., Estroff, L.A. (2013): Evaluation of strengthening mechanisms in calcite single crystals from mollusk shells. *Acta Biomater.*, **9**, 5353–5359.

Lazzeri, M. & De Gironcoli, S. (1998): Ab initio study of Be (0001) surface thermal expansion. *Phys. Rev. Lett.* **81**, 2096

Lazzeri, M., Calandra, M., Mauri, F. (2003): Anharmonic frequency shift in MgB_2. *Phys. Rev. B: Condens. Matter*, **68**, 220509.

Long, X., Ma, Y., Qi, L. (2013): Biogenic and synthetic high magnesium calcite − a review. *J. Struct. Biol.*, **185**, 1–14.

Mavromatis, V., Montouillout, V., Noireaux, J., Gaillardet, J., Schott, J. (2015): Characterization of boron incorporation and speciation in calcite and aragonite from co-precipitation experiments under controlled pH, temperature and precipitation rate. *Geochim. Cosmochim. Acta*, **150**, 299–313.

Menéndez, J. & Cardona, M. (1984): Temperature dependence of the first-order Raman scattering by phonons in Si, Ge, and a-Sn: Anharmonic effects. *Phys. Rev. B: Condens. Matter*, **29**, 2051–2059.

Mitsuguchi, T., Matsumoto, E., Abe, O., Uchida, T., Isdale, P.J. (1996): Mg/Ca thermometry in coral skeletons. *Science*, **274**, 961–963.

Morse, J.W. & Bender, M.L. (1990): Partition coefficients in calcite: Examination of factors influencing the validity of experimental results and their application to natural systems. *Chem. Geol.*, **82**, 265–277.

Murray Roberts, J., Wheeler, A.J., Freiwald, A., Cairns, S.D. (2009): Cold-water corals − the biology and geology of deep-sea coral habitats. Cambridge University Press, New York.

Nguyen, L.T., Rahman, M.A., Maki, T., Tamenori, Y., Yoshimura, T., Suzuki, A., Iwasaki, N., Hasegawa, H. (2014): Distribution of trace element in Japanese red coral Paracorallium japonicum by μ-XRF and sulfur speciation by XANES: Linkage between trace element distribution and growth ring formation. *Geochim. Cosmochim. Acta*, **127**, 1–9.

Noireaux, J., Mavromatis, M., Gaillardet, J., Schott, J., Montouillout, V., Louvat, P., Rollion-Bard, C., Neuville, D.R. (2015): Crystallographic control on the boron isotope paleo-pH proxy. *Earth Planet. Sci. Lett.*, **430**, 398–407.

Palmer, M.R., Pearson, P.N., Cobb, S.J. (1998): Reconstructing past ocean pH-depth profiles. *Science*, **282**, 1468–1471.

Paquette, J. & Reeder, R.J. (1995): Relationship between surface structure, growth mechanism, and trace element incorporation in calcite. *Geochim. Cosmochim. Acta*, **59**, 735–749.

Pavese, A., Catti, M., Price, G.D., Jackson, R.A. (1992): Interatomic potentials for $CaCO_3$ polymorphs (calcite and aragonite), fitted to elastic and vibrational data. *Phys. Chem. Minerals*, **19**, 80–87.

Perdew, J.P., Burke, K., Ernzerhof, M. (1996): Generalized gradient approximation made simple. *Phys. Rev. Lett.*, **77**, 3865–3868.

Pingitore, N.E., Jr, Meitzner, G., Love, K.M. (1995): Identification of sulfate in natural carbonates by X-ray absorption spectroscopy. *Geochim. Cosmochim. Acta*, **59**, 2477–2483.

Prencipe, M., Pascale, F., Zicovich-Wilson, C.M., Saunders, V.R., Orlando, R., Dovesi, R. (2004): The vibrational spectrum of calcite ($CaCO_3$): an ab initio quantum-mechanical calculation. *Phys. Chem. Minerals*, **31**, 559–564.

Quong, A.A. & Liu, A.Y. (1997): First-principles calculations of the thermal expansion of metals. *Phys. Rev. B*, **56**, 7767–7770.

Rao, K.V.K., Naidu, S.V.N., Murthy, K.S. (1968): Precision lattice parameters and thermal expansion of calcite. *J. Phys. Chem. Solids*, **29**, 245–248.

Reeder, R.J., Lamble, G.M., Lee, J.-F., Staudt, W.J. (1994): Mechanism of SeO_4^{2-} substitution in calcite: an XAFS study. *Geochim. Cosmochim. Acta*, **58**, 5639–5646.

Reeder, R.J., Lamble, G.M., Northrup, P.A. (1999): XAFS study of the coordination and local relaxation around Co^{2+}, Zn^{2+}, Pb^{2+}, and Ba^{2+} trace elements in calcite. *Am. Mineral.*, **84**, 1049–1060.

Riccardi, A.L. (2007): Carbonate-associated sulfate: assessment of and use as an isotopic proxy for global sulfur cycling during end-Permian mass extinction. Thesis, The Pennsylvania State University.

Riccardi, A.L., Arthur, M.A., Kump, L.R. (2006): Sulfur isotopic evidence for chemocline upward excursions during the end-Permian mass extinction. *Geochim. Cosmochim. Acta*, **70**, 5740–5752.

Rollion-Bard, C., Blamart, D., Trebosc, J., Tricot, G., Mussi, A., Cuif J.-P. (2011): Boron isotops as a pH proxy: a new look at boron speciation in deep-sea corals using ^{11}B MAS NMR and EELS. *Geochim. Cosmochim. Acta*, **75**, 1003–1012.

Rüggeberg, A., Fietzke, J., Liebetrau, V., Eisenhauer, A., Dullo, W.-C., Freiwald, A. (2008): Stable strontium isotopes ($\simeq^{88/86}$Sr) in cold-water corals − a new proxy for reconstruction of intermediate ocean water temperatures. *Earth Planet. Sci. Lett.*, **269**, 570–575.

Sakurai, T. & Sato, T. (1971): Temperature dependence of vibrational spectra in calcite by means of emissivity measurements. *Phys. Rev. B: Condens. Matter*, **4**, 583–591.

Salje, E.K.H. & Viswanathan, K. (1976): The phase diagram calcite-aragonite as derived from the crystallographic properties. *Contrib. Mineral. Petrol.*, **55**, 55–67.

Salje, E.K.H., Wruck, B., Thomas, H. (1991): Order parameter saturation and low-temperature expansion of Landau theory. *Z. Phys.*, **82**, 399–404.

Salje, E.K.H., Carpenter, M.A., Malcherek, T., Boffa Balaran, T. (2000): Autocorrelation analysis of infrared spectra from minerals. *Eur. J. Mineral.*, **12**, 503–519.

Sen, S., Stebbins, J.F., Hemming, N.G., Ghosh B. (1994): Coordination environments of B impurities in calcite and aragonite polymorphs: a ^{11}B MAS NMR study. *Am. Mineral.*, **79**, 819–825.

Sood, A.K., Arora, A.K., Umadevi, V., Venkataraman, G. (1981): Raman study of temperature dependence of lattice modes in calcite. *Pramana*, **16**, 1–16.

Sterzel, W. & Chorinsky, E. (1968): Die Wirkung schwerer Kohlenstoffisotope auf das Infrarotspektrum von Carbonaten. *Spectrochim. Acta, A: Mol. Biomol. Spectrosc.*, **24**, 353–360.

Stineman, R.W. (1980): A consistently well-behaved method of interpolation. *Creative Comput.*, **6**, 54–57.

Strauss, H. (1999): Geological evolution from isotope proxy signals − sulfur. *Chem. Geol.*, **161**, 89–101.

Takano, B. (1985): Geochemical implications of sulfate in sedimentary carbonates. *Chem. Geol.*, **49**, 393–403.

Takano, B., Asano, Y., Watakuni, K. (1980): Characterization of sulfate ion in travertine. *Contrib. Mineral. Petrol.*, **72**, 197–203.

Tamenori, Y., Yoshimura, T., Luan, N.T., Hasegawa, H., Suzuki, A., Kawahata, H., Iwasaki, N. (2014): Identification of the chemical form of sulfur compounds in the Japanese pink coral (*Corallium elatius*) skeleton using m-XRF/XAS speciation mapping. *J. Struct. Biol.*, **186**, 214–223.

Tang, Y., Elzinga, E.J., Lee, Y.J., Reeder, R.J. (2007): Coprecipitation of chromate with calcite: Batch experiments and X-ray absorption spectroscopy. *Geochim. Cosmochim. Acta*, **71**, 1480–1493.

Valenzano, L., Torres, F.J., Doll, K., Pascale, F., Zicovich-Wilson, C. M., Dovesi, R. (2006): Ab initio study of the vibrational spectrum and related properties of crystalline compounds: the case of $CaCO_3$ calcite. *Z. Phys. Chem.*, **220**, 893–912.

Vavouraki, A., Putnis, C., Putnis, A., Koutsoukos, P. (2008): An Atomic Force Microscopy study of the growth of calcite in the presence of sodium sulfate. *Chem. Geol.*, **253**, 243–251.

Vielzeuf, D., Garrabou, J., Gagnon, A., Ricolleau, A., Adkins, J., Gunther, D., Hametner, K., Devidal, J. L., Reusser, E., Perrin, J., Floquet, N. (2013): Distribution of sulphur and magnesium in the red coral. *Chem. Geol.*, **355**, 13−27.

Wasylenki, L.E., Dove, P.M., Wilson, D.S., De Yoreo, J.J. (2005): Nanoscale effects of strontium on calcite growth: an in situ AFM study in the absence of vital effect. *Geochim. Cosmochim. Acta*, **69**, 3017–3027.

Weiner, S. & Dove, P.M. (2003): An overview of biomineralization processes and the problem of the vital effect. *Rev. Mineral. Geochem.*, **54**, 1–29.

White, W.B. (1974): The carbonate minerals. *in* "The infrared spectra of minerals", V.C. Farmer, ed. Mineralogical Society, London, 227–284.

Xu, B. & Poduska, K.M. (2014): Linking crystal structure with temperature-sensitive vibrational modes in calcium carbonate minerals. *Phys. Chem. Chem. Phys.*, **16**, 17634.

Yi, H., Balan, E., Gervais, C., Segalen, L., Fayon, F., Roche, D., Person, A., Morin, G., Guillaumet, M., Blanchard, M., Lazzeri, M., Babonneau, F. (2013): A carbonate-fluoride defect model for carbonate-rich fluorapatite. *Am. Mineral. (letter)*, **98**, 1066–1069.